Refinement of the T466 Prototype Tungsten/Scintillating Fiber Electromagnetic Calorimeter

Evan Kirby Oleg Tsai

23 August 2003

Abstract

In April 2003, UCLA researchers conducted test run T466 at the Stanford Linear Accelerator Center with their newly designed electromagnetic calorimeter towers composed of tungsten powder and scintillating fibers. The prototype's energy resolution, uniformity of response, and linearity were measured using an electron beam with a momentum of up to 10 GeV. The measured energy resolution was $17\%/\sqrt{E}$. This report will summarize the basic concepts of high energy calorimetry, suggest possible methods to improve resolution, and propose quality control methods to test improved towers.

1 Introduction to Calorimetry

The primary purpose of a calorimeter in high energy physics is to measure the energy of an incident particle. Secondarily, a calorimetry array can provide position information and particle identification [1]. Usually, the calorimeter fully absorbs the energy of the incoming particle. The calorimeter measures either the ionization created by the particle or its Čerenkov light. The final signal is proportional to the primary particle energy. Calorimeters are specialized to detect electromagnetic particles—photons, electrons, and positrons—or hadrons. This report focuses on electromagnetic calorimeters (EMCs).

1.1 Homogeneous vs. sampling calorimeters

Calorimeters consist of a single, continuous medium (homogeneous calorimeters) or alternating layers of dense, passive material and light, active material (sampling calorimeters). Homogeneous calorimeters usually exhibit better energy resolution than sampling calorimeters. However, the material in a homogeneous calorimeter must transport the energy information to the detector. The availability of such materials limits the range of acceptable

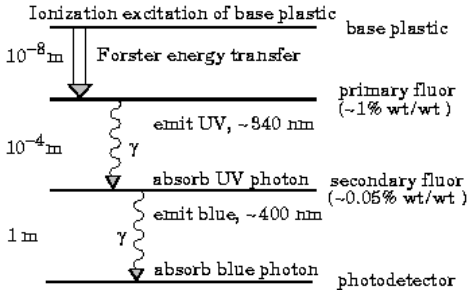

Figure 1: An energy ladder diagram showing the transfer of particle energy to detectable photons in a plastic scintillator. The numbers on the left give the length scale of the energy transfer, and the numbers on the right give the concentration of each fluor by weight. Figure taken from [2].

media. On the other hand, the passive medium in a sampling calorimeter need not carry information. The high-Z passive medium catalyzes energy deposition while the active medium samples that energy. The flexibility in the choice of a passive absorber allows sampling calorimeters to cost at least ten times less than homogeneous calorimeters.

In general, a more compact calorimeter is a better calorimeter. The spatial density, or granularity, of a calorimetry array determines its spatial resolution: A more compact array more easily distinguishes one particle from another. Futhermore, compact calorimeters require less material; thus, they are less expensive. Ultimately, the type of array determines the type of calorimeter. So far, the homogeneous stolzite ($PbWO_4$) calorimeter for the Compact Muon Solenoid is the most compact EMC. The Hadron/Electron Ring Accelerator uses a quite compact sampling tungsten/silicon calorimeter. The Next Linear Collider collaboration also is considering such an EMC.

1.2 Operating principles of the sampling EMC

When high-energy particles interact with matter, they lose energy. Electrons and positrons decelerate and radiate photons, and photons produce electron-positron pairs. Eventually, the incident particle produces tens of thousands of lower energy particles. This process is called an electromagnetic shower. Because the active medium of a sampling detector comprises a small fraction of the total material in the detector, the passive medium determines the profile of the shower.

A popular choice of active medium for the sampling EMC is the plastic scintillator. High-energy particles lose energy to photon production in a scintillating medium. Figure 1 displays the complete process. The incident particle ionizes a plastic base. The deexcitation of electrons in the base

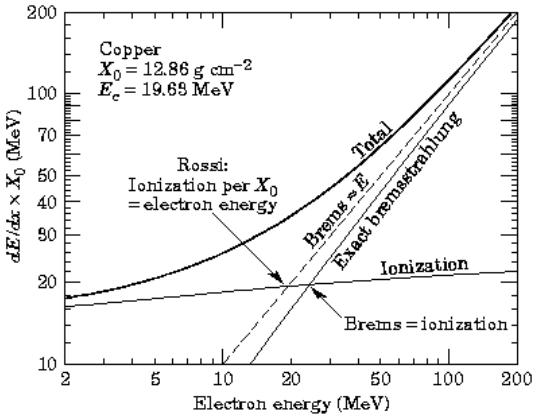

Figure 2: The energy loss of electrons in copper versus kinetic energy. Bremsstrahlung radiation is approximately proportional to the energy of the particle, but the exact relation is also shown. The critical energy is the point at which losses due to Bremsstrahlung radiation are equal to losses due to ionization. Figure taken from [2].

produces ultraviolet photons. However, the attenuation length in the base plastic for these photons is short. A fluor absorbs the energy from the ionization in a resonant dipole-dipole process called the Forster interaction, and it reemits photons at a wavelength with a longer attenuation length. Sometimes secondary or tertiary fluors serve to adjust the wavelength of the photons to further increase the attenuation length. The numbers of photons produced depends on the energy the incident particle deposits in the medium. In an assembled EMC, a photodetector collects these photons and converts them into a current pulse. The total charge in this pulse is proportional to the energy of the primary particle. Typical photodetectors include avalanche photodiodes, such as those used in the T466 experiment, and PIN (p-type-insulator-n-type) diodes.

Another type of EMC is a Čerenkov detector. When a particle exceeds the speed of light in a medium, it produces an electromagnetic shock wave called Čerenkov light. A material with a high index of refraction has a low threshold for the particle energy required to create Čerenkov light. In a Čerenkov detector, a high-n material such as lead glass maximizes the Čerenkov light, which a photodetector measures.

1.3 Electromagnetic shower development

As an incident electron, positron, or photon-produced particle pair passes through matter, it decelerates and therefore radiates. This Bremsstrahlung

(German for "braking") radiation is the primary mode of energy release for high energy electrons and positrons. Only when the particles lose most of their energy does ionization dominate as the main contributor to energy deposition. The energy at which energy loss from both modes are equal is called the critical energy. Figure 2 displays the total energy loss of electrons passing through matter and the two major contributors to that energy loss. A good approximation to the critical energy is $\epsilon_c \approx \frac{(800\ \mathrm{MeV})}{Z+1.2}$ where Z is the atomic number of the absorber. An approximation to energy loss is $\frac{\mathrm{d}E}{\mathrm{d}x} \approx -\frac{E}{X_0}$. The value X_0 is the radiation length of the medium, the distance in which an electron loses all but $1/e$ of its incident energy. X_0 is given by the approximation

$$X_0 \approx \frac{(716.4\ \mathrm{g \cdot cm^{-2}})A}{Z(Z+1)\ln(287/\sqrt{Z})} \tag{1}$$

where A is the atomic weight of the absorber. The attenuation length for a photon is close to the radiation length: $X_\gamma \approx \frac{9}{7}X_0$ [3]. The similar lengths make electromagnetic showers simple to describe relative to hadronic showers.

It is convenient to express all lengths in terms of X_0. Most of the dependence on choice of absorber then disappears from the equations of energy deposition. For example, energy loss along the longitudinal axis in terms of the incident energy, E_0, is given by a relation involving the gamma function:

$$\frac{\mathrm{d}E}{\mathrm{d}t} \approx E_0 b\Big(\frac{(bt)^{a-1}\mathrm{e}^{-bt}}{\Gamma(a)}\Big) \tag{2}$$

where t is the depth in radiation lengths and a and b are properties of the material. b is typically between 0.4 and 0.7 and a is given by the relation

$$t_{\max} = \frac{a-1}{b} \approx \ln(\frac{E_0}{\epsilon_c}) + C_i \qquad i = \mathrm{e}, \gamma \tag{3}$$

$$C_i = \begin{cases} -0.5 & i = \mathrm{e} \\ +0.5 & i = \gamma \end{cases} \tag{4}$$

$t_{\max}$ is the longitudinal depth in radiation lengths of maximum energy deposition. It provides a means to extrapolate the depth that contains some fraction of the total energy deposited into the medium. For example, a particle loses 95% of its energy in a depth

$$t_{95\%} \approx t_{\max} + 0.08Z + 9.6 \tag{5}$$

A unit called the Molière radius, ρ_M, more conveniently describes the transverse development of the shower.

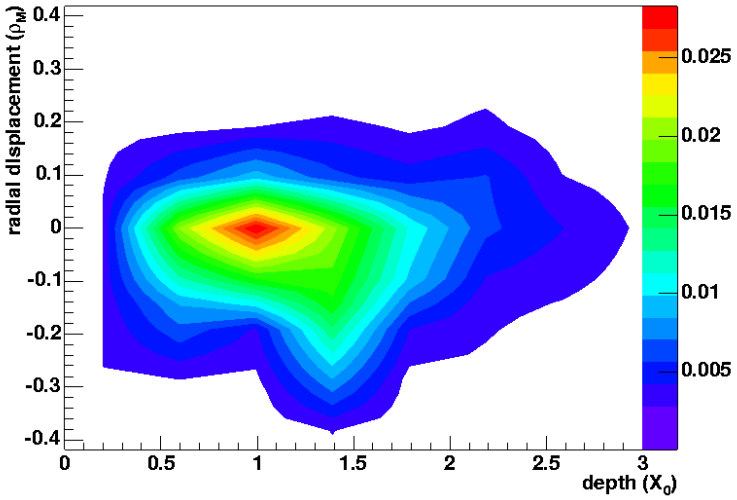

Figure 3: Experimentally determined energy deposition in lead from a 1 GeV electron beam. The contours display the percentage of total deposition. Energy deposition is roughly independent of the absorbing material when plotted in terms of X_0 and ρ_M. Data taken from [4].

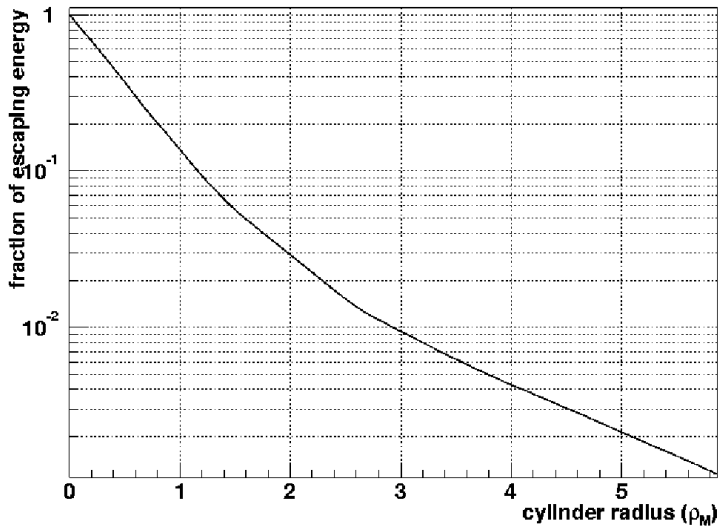

Figure 4: Experimentally determined fraction of energy escaping a long cylinder. Radial units are the Molière radius. Data taken from [4].

$$\rho_M = X_0 \frac{E_S}{\epsilon_c} \quad (6)$$

$$E_S = m_e c^2 \sqrt{\frac{4\pi}{\alpha}} \approx 21.2\text{MeV} \quad (7)$$

where α is the QED coupling (fine structure) constant. A cylinder of a Molière radius whose axis is the initial direction of the incident particle contains about 90% of the shower's energy. Figures 3 and 4 show the results of a 1966 experiment [4] that examined energy deposition in various materials.

1.4 EMC energy resolution

Photostatistics fundamentally limits the energy resolution of a scintillating EMC. Because the number of photons produced increases with energy, energy resolution also increases with energy. The general formula for energy resolution is

$$\frac{\sigma(E)}{E} = \frac{a}{\sqrt{E}} \oplus b \quad (8)$$

($\oplus$ denotes addition in quadrature: $x \oplus y = \sqrt{x^2 + y^2}$.) Fluctuations in particle pair production provide a fundamental limit of energy resolution, represented by a. Imperfections in the design of a particular calorimeter determine b.

2 The T466 EMC Towers

The research and development goal of the T466 project is to create an efficient method of producing high-granularity, compact sampling EMCs. The project aims for an energy resolution of $10\%/\sqrt{E}$ or less and a radiation length as small as possible. The production method should be simple and cost-effective. Scintillating fiber technology with a tungsten converter best fits the project goals. After the test run at SLAC, UCLA researchers conducted a follow-up investigation into the energy resolution of the prototype EMCs in June, July, and August 2003.

The T466 prototype EMC is a 22 mm × 22 mm × 120 mm tower. The active medium consists of 500 scintillating fibers staggered at 1.0 mm intervals packed in 11.1 g/cm^2 tungsten powder. The far end of the tower consists of a light mixer that directs the light from all the fibers onto a PMT. The incident edge of the tower is a mirror intended to increase signal acceptance by reflecting photons reemitted by the fluor in the fibers back to the PMT. In the detector, the tower is oriented at 3° relative to the incoming beam to avoid a particle traveling through a low-Z scintillating fiber

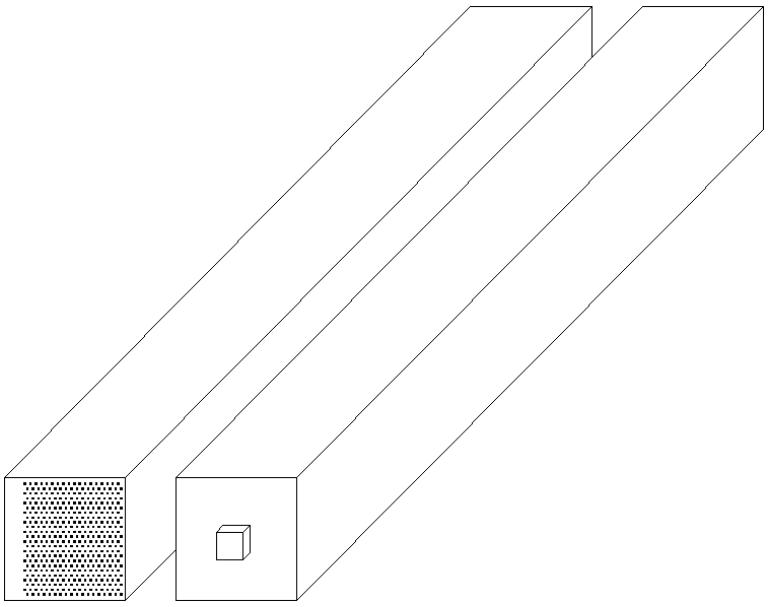

Figure 5: T466 EMC towers. The left tower shows the incident face, where the square scintillating fibers are visible through the mirror. The right tower shows the back face, where the light mixer emerges from the brass container. The PMT abuts this protrusion.

without interacting, a phenomenon called "channeling." The fundamental resolution limit, a, for these towers is around 15%. Nonuniformities in the powder density, in the fiber spacing, and in the light mixing may worsen the energy resolution. The radiation length, given by (1), is 6.09 mm. The Molière radius, given by (7), is 10 mm. Thus, approximately 544 fibers—more than in a single tower—are needed to contain 90% of the energy of one electromagnetic shower. That number increases to 2176 fibers to contain 98% of the energy.

In production, the fibers were packed into a rectangular brass container with 0.127 mm walls using a mesh. As the mesh was pulled up to the top of the container, tungsten powder sifted through it to fill the space between the fibers. After the tower filled, the sides bulged in the center by about 0.5 mm. The towers were compressed back to a rectangular shape. If the tungsten power is not particularly fluid, the fibers possibly shifted toward the center of the tower, creating unresponsive regions near the walls at the longitudinal center of the tower. The test run at SLAC supported this hypothesis with a signal drop by a factor of two at a point between two side-by-side towers.

2.1 Influence of tungsten powder on fiber response

The first tests investigated the effect of the tungsten powder on the response of the fibers. Three sources independently excited the fibers at the mirror end of a tower: a 350 nm LED, a 370 nm LED, and a collimated beta source, ^{90}Sr. (Read below for a description of the strontium source.) The LED profiles approximated an electromagnetic shower profile in the test run at SLAC. The sources illuminated the towers at 66 points on a 5 mm $\times$ 10 mm grid near the central axis of the tower. The RMSs of the spatial distributions of PMT response were greater than those of the test run. Variations in the apertures of the fibers may explain the larger RMS. This effect would not appear in an actual electromagnetic shower, but the grid scans would be quite sensitive to it. If this method is to be used for quality control, the fibers must be well-aligned.

An identical scan over a tower without tungsten revealed no significant difference in the RMS of the distribution. Therefore, the presence of tungsten powder does not significantly affect the light response of the fibers. However, the experiment scanned only the center of the tower. Future tests may explore the effect of tungsten powder on the fibers near the edges of the tower.

2.2 Light mixer uniformity tests

The next experiment tested the light mixer's uniformity. Light from a stack of ultraviolet LEDs passed through a 0.5 mm slit flush with the face of the tower. The slit was intended to illuminate a single row of fibers. The

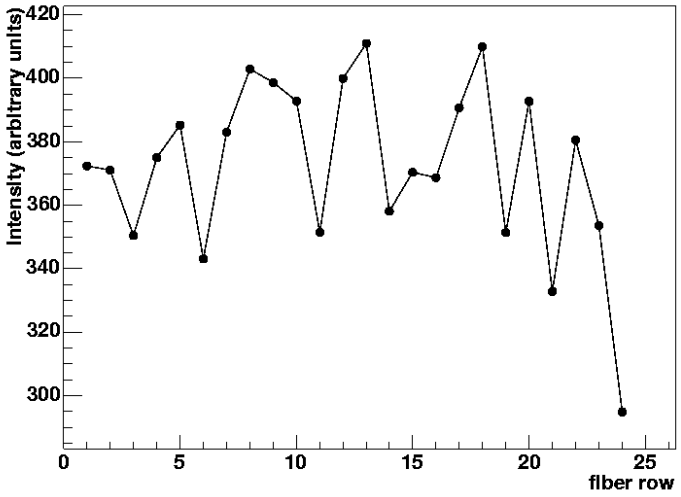

Figure 6: The measured intensity from a stack of ultraviolet LEDs from each row of scintillating fibers.

LEDs sometimes illuminated an adjacent row of fibers. Therefore, misaligned fibers are the primary contributors to variation in light response in this test. Some signal drop was observed near the edges of the tower (see figure 6), but the brass foil container partially obscured the row of fibers that exhibited the signal drop. The light mixer performs uniformly with respect to fiber position to within 10%. It is not responsible for the signal drop between towers observed in the test run at SLAC.

2.3 Fiber distribution uniformity tests

The final experiment probed the thickness of the tungsten powder at the edges of the container. An increasing number of brass foils attenuated the beta beam from the ^{90}Sr source collimated onto the longitudinal center of the tower. Figure 7 shows the results. They determine the relation that allows the reconstruction of dead layer thickness from the counting rate of ^{90}Sr.

The light output from a scintillating fiber depends on the pressure exerted on the fiber, as demonstrated by the H1 collaboration. ^{60}Co, a source immune to absorption in the small amount of tungsten powder, probed this effect. ^{60}Co is a gamma source, meaning that it emits mono-energetic high-energy photons from the deexcitation of nuclei. It emits 1.173 MeV and 1.33 MeV photons (gamma particles). At these energies, the small variations in the depth of the tungsten powder do not significantly attenuate the number

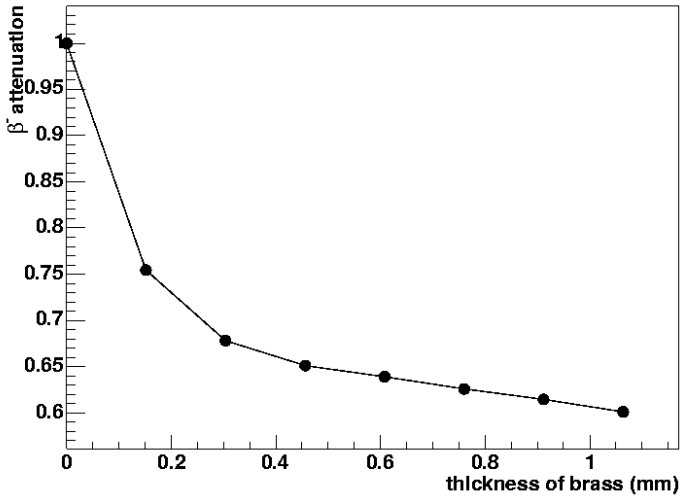

Figure 7: The attenuation in the counting rate of β^- from ^{90}Sr versus the thickness of brass between the source and the tower.

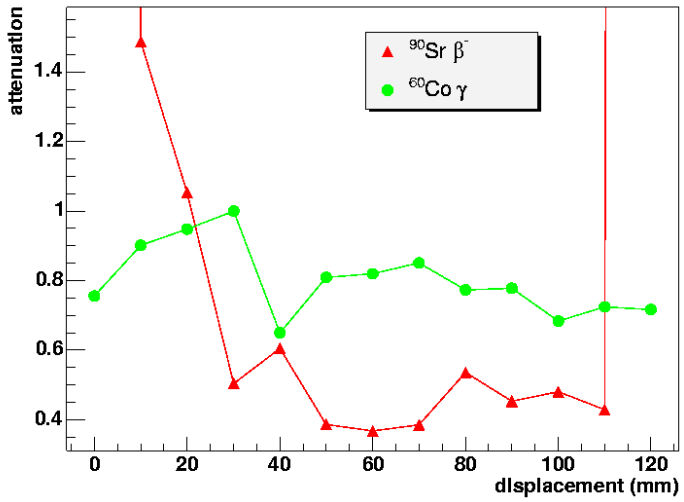

Figure 8: The attenuation in the counting rates from ^{60}Co and ^{90}Sr versus longitudinal displacement along the tower.

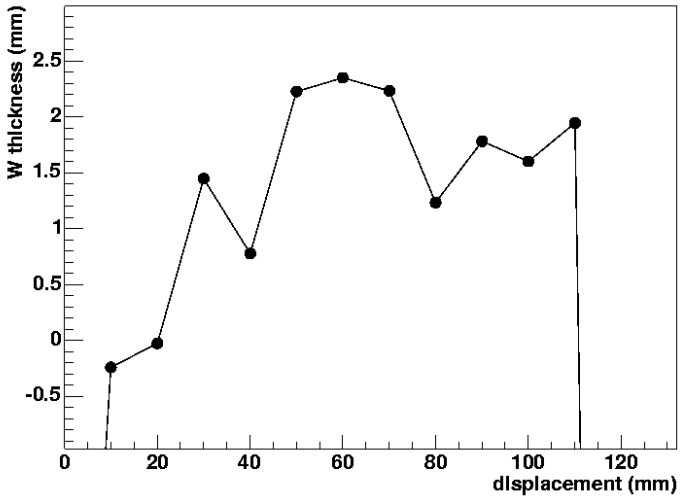

Figure 9: The experimentally determined estimate of the variation in tungsten powder thickness.

of photons. The response of the tower to ^{60}Co versus position along the tower provides a background adjustment.

^{90}Sr on the other hand is quite susceptible to small variations in the depth of the tungsten powder. It is a beta source, meaning that it emits electrons in a continuous spectrum of energy. The responsible nuclear decay is $n \rightarrow p + e^- + \bar{\nu}_e$. Momentum sharing between the proton, the electron, and the neutrino creates the continuous energy spectrum of the beta particles. The approximate upper limit for the beta energy of ^{90}Sr is 0.546 MeV. Figure 8 displays the attenuation of both radioactive sources versus longitudinal displacement along the tower.

Figures 7 and 8 theoretically provide all the data necessary to determine the thickness of the tungsten powder at each point the radioactive sources probed. However, the experiment is quite imprecise. First, the terminal ends of the fibers contribute edge effects to the counting rate near the first and last points of the graph, especially for ^{90}Sr. Second, none of the points taken is an absolute counting rate—one taken in the absence of tungsten. The attenuation shown in figure 8 is normalized to 1 at the maximum counting rate for ^{60}Co and to 1 at a counting rate guessed to be the maximum without edge effects for ^{90}Sr. The choice of normalization can disturb the calculation of the tungsten thickness signficantly. Figure 9 shows the unlikely results of the calculation. The negative thickness is an artifact of the edge effects. The maximum possible thickness of the tungsten at the center of the tower is 0.5 mm.

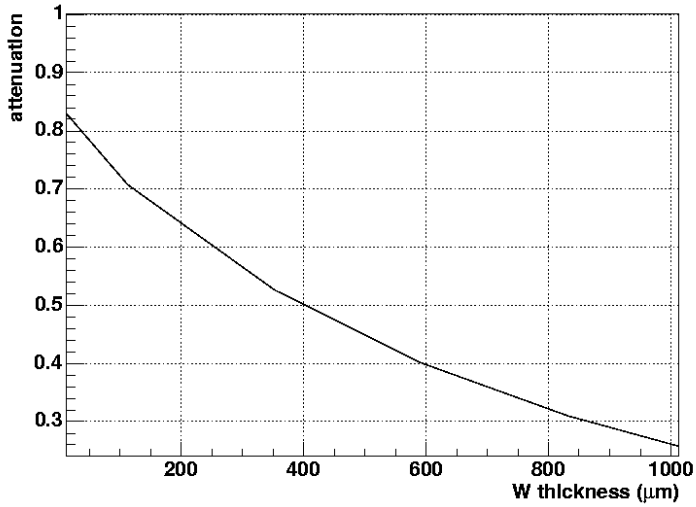

Figure 10: Inferred electron attenuation versus tungsten thickness using data from [4].

This experiment may be refined. The edge effects may be explored by placing two towers well matched in light response face-to-face. The response of each tower should be continuous and smooth as a radioactive source is scanned over the interface between the two towers. A sharp peak in respsonse will give the magnitude of the edge effects. Also, measuring the counting rate of ^{90}Sr on an empty tower not filled with tungsten will provide an absolute counting rate to which the counting rates with tungsten may be normalized. Finally, it would be useful to have a well-collimated, mono-energetic source of electrons. The current ^{90}Sr collimator still allows quite a bit of off-center leakage, which creates a significant background. A monoharminator, a device that selects a narrow energy range of electrons and filters out the rest, would increase the precision of the scans involving beta sources. Unfortunately, they are large, heavy, and difficult to construct because they require a strong magnet.

Reference [4] provides a useful method to determine the tungsten thickness indirectly. The most alarming result from the T466 test run was the factor of two attenuation between two towers. Numerical integration using Nelson's tabulated energy deposition over the volume of the towers with a successively larger rectangular gap omitted from calculation yields figure 10. The attenuation at zero thickness is not unity because the 127 μm brass wall of the container provides an additional dead area. The point at which the signal is attenuated by a factor of 2 is 410 μm of tungsten. This number is an underestimate of the maximum tungsten thickness because it assumes

a dead area in the shape of a rectangular prism of uniform depth. A more accurate shape would be much thinner near the ends of the towers, and it would bulge in the middle.

3 Recommendations

The resolution experiments on the T466 EMC towers conducted in summer 2003 have determined that the tungsten powder is not as fluid as originally expected. The packing method shifts the fibers in such a way as to create an unresponsive dead region. The signal attenuation between the towers must be eliminated before the resolution will approach an acceptable level. The best way to improve uniformity of response is to develop a method of packing the tungsten powder that maintains a uniform distribution of fibers. Furthermore, the tower must be made rigid by infusing epoxy into the final assembly. Finally, the resolution may be improved by increasing the fraction of active material.

References

[1] P. B. Cushman. F. Sauli, ed. *Instrumentation in High Energy Physics.* Singapore: World Scientific, 1992.

[2] K. Hagiwara *et. al.*, Phys. Rev. **D66**, 010001 (2002).

[3] W. R. Leo. *Techniques for Nuclear and Particle Physics Experiments: A How-To Approach.* Heidelberg: Springer-Verlag, 1994.

[4] W. R. Nelson, T. M. Jenkins, R. C. McCall, and J. K. Cobb, Phys. Rev. **149**, 201 (1966).